

Rough-Terrain Locomotion and Unilateral Contact Force Regulations With a Multi-Modal Legged Robot

Kaier Liang, Eric Sihite, Pravin Dangol, Andrew Lessieur, and Alireza Ramezani¹

Abstract—Despite many accomplishments by legged robot designers, state-of-the-art bipedal robots are prone to falling over, cannot negotiate extremely rough terrains and cannot directly regulate unilateral contact forces. Our objective is to integrate merits of legged and aerial robots in a single platform. We will show that the thrusters in a bipedal legged robot called *Harpy* can be leveraged to stabilize the robot’s frontal dynamics and permit jumping over large obstacles which is an unusual capability not reported before. In addition, we will capitalize on the thrusters action in *Harpy* and will show that one can avoid using costly optimization-based schemes by directly regulating contact forces using an Reference Governor (RGs). We will resolve gait parameters and re-plan them during gait cycles by only assuming well-tuned supervisory controllers. Then, we will focus on RG-based fine-tuning of the joints desired trajectories to satisfy unilateral contact force constraints.

I. INTRODUCTION

Raibert’s hopping robots [1] and Boston Dynamics’ robots [2] are amongst the most successful examples of legged robots, as they can hop or trot robustly even in the presence of significant unplanned disturbances. Other than these successful examples, a large number of underactuated and fully actuated bipedal robots have also been introduced. Agility Robotics’ Cassie [3], Honda’s ASIMO [4] and Samsung’s Mahru III [5] are capable of walking, running, dancing and going up and down stairs, and the Yobotics-IHMC [6] biped can recover from pushes. Despite these accomplishments, all of these systems are prone to falling over and cannot negotiate extremely rough terrains. Even humans, known for their natural, dynamic and robust gaits cannot recover from severe rough terrain perturbations, external pushes or slippage on icy surfaces. Our goal is to enhance the robustness of these systems through a distributed array of thrusters and nonlinear control.

In this paper, we will report our efforts in designing closed-loop feedback for the thruster-assisted walking of a legged system called *Harpy* (shown in Fig. 1), currently its hardware being developed at Northeastern University. This biped is equipped with a total of eight actuators, and a pair of coaxial thrusters fixed to its torso. Our motivation stems from the merits of aerial and legged systems and we intend to integrate these merits in a single platform. Contrary to fixed- or rotary-wing aerial systems, legged robots cannot exhibit a fast mobility and fly over obstacles. A legged robot’s capability to negotiate extremely bumpy terrains (e.g., semi-collapsed buildings in the aftermath of an earthquake) is

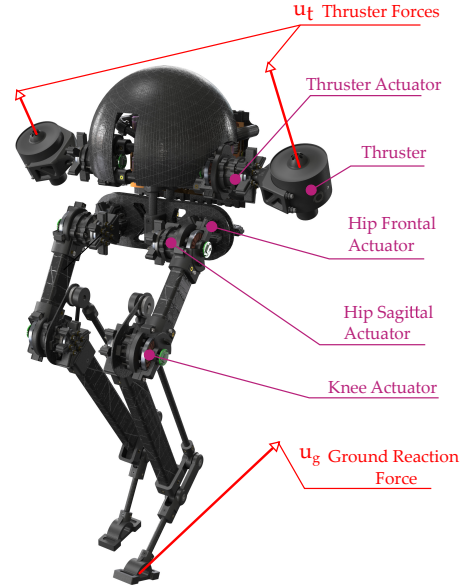


Fig. 1. Illustration of a concept design for *Harpy*, a thruster-assisted bipedal robot designed by the authors to study robust, efficient and agile legged robotics.

very limited in that, for example, the height of terrain bumps should not exceed the size of the legs [7], [8], [9]. However, a legged robot maintains a superior energetic efficiency of locomotion because its overall body weight is supported by the legs, can safely operate inside buildings and has no sharp, rotating blades to cause severe laceration injuries to humans.

Thruster-assisted legged locomotion has not been explored previously except to a limited extent in a few examples that only considered the hardware-related challenges [10]. These robots potentially can offer rich and challenging dynamics and control problems. The overactuation and control allocation problems led by the coexistence of thrusters and joint actuators not only can provide opportunities to study interesting control ideas, but also, from a dynamical behavior standpoint, can permit studying unexplored behaviors such as walking under buoyancy phenomena [11]. Also, studying multi-modal systems that can switch from one mode to another in order to overcome the demanding mobility objectives in unstructured environments is a rather new research problem and potentially can result in interesting machine-learning and optimization-based motion planning problems [12].

From a feedback design standpoint, the challenge of simultaneously providing asymptotic stability and gait feasibility constraints satisfaction in legged systems have been exten-

¹SiliconSynapse Laboratory, ECE Department, Northeastern University, Boston, MA, USA. emails: {liang.k, e.sihite, dangol.p, lessieur.a, a.ramezani} @northeastern.edu

sively addressed [13]. For instance, the method of Hybrid Zero Dynamics (HZD) has provided a rigorous model-based approach to assign attributes such as efficiency of locomotion in an off-line fashion. Other attempts entail optimization-based, nonlinear approaches to secure safety and performance of legged locomotion [14], [15], [16], [17], [18], [19].

Thrusters can result in unparalleled capabilities. For instance, gait trajectory planning (or re-planning), control and unilateral contact force regulation can be treated significantly differently as we have shown previously [20], [21], [22] and will further discuss new details in this paper. That said, real-time gait trajectory design in legged robots has been widely studied and the application of optimization-based methods is very common [23]. In general, in these paradigms, an optimization-based controller adjusts the gait parameters throughout the whole gait cycle such that not only the robot's posture is adjusted to accommodate the unplanned posture adjustments but also the joints position, velocity and acceleration are modified to avoid slipping into infeasible scenarios, e.g., the violation of contact forces. What makes these methods further cumbersome is that they are widely defined based on Whole Body Control (WBC) which can lead to computationally expensive algorithms [24].

These problems are widely known to suffer from curse of dimensionality and other popular paradigms such as Approximate Dynamic Programming (ADP) [25], Reinforcement Learning (RL) [26], decoupled approaches to design control for nonlinear stochastic systems [27], etc., can potentially remedy the challenges. However, these approaches are far from providing any practical solutions to the problem in hand and they are shown to be only effective on simpler practical robots mainly those that can only demonstrate quasi-static gaits.

We will capitalize on the thrusters action in Harpy and will show that one can limit the use of costly optimization-based schemes by directly regulating contact forces. We will resolve gait parameters and re-plan them during the whole Single Support (SS) phase, which is the longest phase in a gait cycle, by only assuming well-tuned supervisory controllers found in [28], [29], [30] and by focusing on fine-tuning the joints desired trajectories to satisfy unilateral contact force constraints. To do this, we will devise intermediary filters based on the celebrated idea of Explicit Reference Governors (ERG) [31], [32], [33], [34]. ERGs relied on provable Lyapunov stability properties can perform the motion planning problem in the state space in a much faster way than widely used optimization-based methods. That said, these ERG-based gait modifications and impact events (i.e., impulsive effects) can lead to severe deviations from the desired periodic orbits and standard legged robots cannot sustain these perturbations. Previously, we demonstrated that the thrusters can be leveraged to enforce hybrid invariance in a robust fashion by applying predictive schemes within the Double Support (DS) phase [22]. Last, we also will show that thrusters can be leveraged to stabilize frontal dynamics and permit jumping over large obstacles which is an unusual capability not reported before.

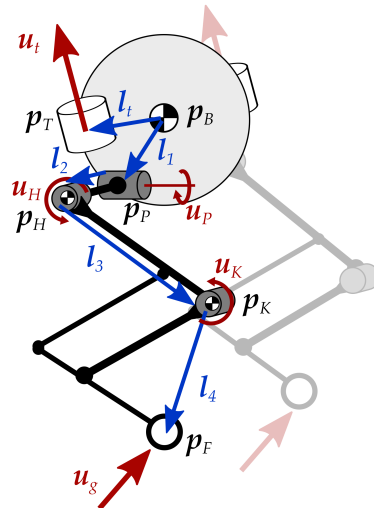


Fig. 2. Shows the joint movements, key positions (p_i) and dimensions (l_i) of Harpy. The non-conservative forces and torques acting on the system are denoted by u_i .

This paper is outlined as follows: the dynamic modeling for Harpy and the reduced-order models which will be used in the numerical simulation and controller design, the discussion on thruster assisted locomotion, numerical simulation discussions, and then followed by the concluding remarks.

II. DYNAMIC MODELING OF HARPY

This section outlines the dynamics formulation of the robot which is used in the numerical simulation in Section IV, in addition to the reduced order models which are used in the controller design. Fig. 2 shows the kinematic configuration of Harpy which listed the center of mass (CoM) positions of the dynamic components, joint actuation torques, and thruster torques. The system model has a combined total of 12 degrees-of-freedom (DoFs): 6 for the body and 3 on each leg. Due to the symmetry, the left and right side of the robot follow a similar derivations so only the general derivations are provided in this section.

A. Euler-Lagrange Formalism

The Harpy equations of motion are derived using Euler-Lagrangian dynamics formulation. In order to simplify the system, each linkages are assumed to be massless and the mass are concentrated at the body and the joint motors. Consequently, the lower leg kinematic chain is considered to be massless which significantly simplifies the system. The three leg joints are labeled as the hip frontal (pelvis P), hip sagittal (hip H) and knee sagittal (knee K), as illustrated in Fig. 2. The thrusters are also considered to be massless and capable of providing forces in any directions to simplify the problem.

Let γ_h be the frontal hip angle while ϕ_h and ϕ_k be the sagittal hip and knee angles respectively. Let the superscript $\{B, P, H, K\}$ represent the frame of reference about the body, pelvis, hip, and knee while the inertial frame is represented without the superscript. Let R_B be the rotation matrix

from the body frame to the inertial frame (i.e. $\mathbf{x} = R_B \mathbf{x}^B$). The pelvis motor mass is added to the body mass. Then the positions of the hip and knee CoM are defined using kinematic equations:

$$\begin{aligned} \mathbf{p}_P &= \mathbf{p}_B + R_B \mathbf{l}_1^B, & \mathbf{p}_H &= \mathbf{p}_P + R_B R_x(\gamma_h) \mathbf{l}_2^P \\ \mathbf{p}_K &= \mathbf{p}_H + R_B R_x(\gamma_h) R_y(\phi_h) \mathbf{l}_3^H, \end{aligned} \quad (1)$$

where R_x and R_y are the rotation matrices about the x and y axis respectively, \mathbf{l} is the length vectors representing the conformation of Harpy which are constant in their respective local frame of reference. The foot and thruster positions are defined as:

$$\begin{aligned} \mathbf{p}_F &= \mathbf{p}_K + R_B R_x(\gamma_h) R_y(\phi_h) R_y(\phi_k) \mathbf{l}_4^K \\ \mathbf{p}_T &= \mathbf{p}_B + R_B \mathbf{l}_t^B \end{aligned} \quad (2)$$

where the length vector from the knee to the foot is $\mathbf{l}_4^K = [-l_{4a} \cos \phi_k, 0, -(l_{4b} + l_{4a} \sin \phi_k)]^\top$ which is the kinematic solution to the parallel linkage mechanism of the lower leg. Let $\boldsymbol{\omega}_B$ be the angular velocity of the body. Then the angular velocities of the hip and knee are defined as: $\boldsymbol{\omega}_H^B = [\dot{\gamma}_h, 0, 0]^\top + \boldsymbol{\omega}_B^B$ and $\boldsymbol{\omega}_K^H = [0, \dot{\phi}_h, 0]^\top + \boldsymbol{\omega}_H^H$.

Finally, the energy of the system for the Lagrangian dynamics formulation are defined as follows:

$$\begin{aligned} K &= \frac{1}{2} \sum_{i \in \mathcal{F}} \left(m_i \mathbf{p}_i^\top \mathbf{p}_i + \boldsymbol{\omega}_i^{i^\top} \hat{I}_i \boldsymbol{\omega}_i^i \right) \\ V &= - \sum_{i \in \mathcal{F}} \left(m_i \mathbf{p}_i^\top [0, 0, -g]^\top \right), \end{aligned} \quad (3)$$

where $\mathcal{F} = \{B, H_L, K_L, H_R, K_R\}$ are the relevant frame of references and mass components (body, hip and knee of each side), and the subscripts L and R represent the left and right side of the robot. Furthermore, \hat{I}_i is the inertia about its local frame, and g is the gravitational constant. This forms the Lagrangian of the system $L = K - V$ which is used to derive the system's Euler-Lagrangian equations of motion. The dynamics of the body angular velocity is derived using the modified Lagrangian for rotation in $SO(3)$ to avoid using Euler angles and the potential gimbal lock associated with them. This results in the following equations of motion following Hamilton's principle of least action:

$$\begin{aligned} \frac{d}{dt} \left(\frac{\partial L}{\partial \boldsymbol{\omega}_B^B} \right) + \boldsymbol{\omega}_B^B \times \frac{\partial L}{\partial \boldsymbol{\omega}_B^B} + \sum_{j=1}^3 \mathbf{r}_{Bj} \times \frac{\partial L}{\partial \mathbf{r}_{Bj}} &= \mathbf{u}_1 \\ \frac{d}{dt} \left(\frac{\partial L}{\partial \dot{\mathbf{q}}} \right) - \frac{\partial L}{\partial \mathbf{q}} &= \mathbf{u}_2, & \frac{d}{dt} R_B &= R_B [\boldsymbol{\omega}_B^B]_\times, \end{aligned} \quad (4)$$

where $[\cdot]_\times$ is the skew operator, $R_B^\top = [\mathbf{r}_{B1}, \mathbf{r}_{B2}, \mathbf{r}_{B3}]$, $\mathbf{q} = [\mathbf{p}_B^\top, \gamma_{h_L}, \gamma_{h_R}, \phi_{h_L}, \phi_{h_R}]^\top$ is the dynamical system states other than $(R_B, \boldsymbol{\omega}_B^B)$, and \mathbf{u} is the generalized forces. The knee sagittal angle ϕ_k which is not associated with any mass is updated using the knee joint acceleration input $\mathbf{u}_k = [\ddot{\phi}_{k_L}, \ddot{\phi}_{k_R}]^\top$. Then the system acceleration can be derived as follows:

$$M\mathbf{a} + \mathbf{h} = B_j \mathbf{u}_j + B_t \mathbf{u}_t + B_g \mathbf{u}_g \quad (5)$$

where $\mathbf{a} = [\ddot{\boldsymbol{\omega}}_B^B, \ddot{\mathbf{q}}, \ddot{\phi}_{k_L}, \ddot{\phi}_{k_R}]^\top$, \mathbf{u}_t is the thruster force, $\mathbf{u}_j = [u_{P_L}, u_{P_R}, u_{H_L}, u_{H_R}, \mathbf{u}_k^\top]^\top$ is the joint actuation, and

\mathbf{u}_g is the ground reaction forces (GRFs). The variables M , \mathbf{h} , B_t , and B_g are a function of the full system states:

$$\mathbf{x} = [\mathbf{r}_B^\top, \mathbf{q}^\top, \phi_{K_L}, \phi_{K_R}, \boldsymbol{\omega}_B^{B^\top}, \dot{\mathbf{q}}^\top, \dot{\phi}_{K_L}, \dot{\phi}_{K_R}]^\top, \quad (6)$$

where the vector \mathbf{r}_B contains the elements of R_B . Using $B_j = [0_{6 \times 6}, I_{6 \times 6}]$ allows \mathbf{u}_j to actuate the joint angles directly. Let $\mathbf{v} = [\boldsymbol{\omega}_B^{B^\top}, \dot{\mathbf{q}}^\top]^\top$ be the velocity of the generalized coordinates, then B_t and B_g can be defined using the virtual displacement from the velocity as follows:

$$B_t = \begin{bmatrix} \left(\frac{\partial \dot{\mathbf{p}}_{T_L} / \partial \mathbf{v}} \right)^\top \\ \left(\frac{\partial \dot{\mathbf{p}}_{T_R} / \partial \mathbf{v}} \right)^\top \\ 0_{2 \times 6} \end{bmatrix}, \quad B_g = \begin{bmatrix} \left(\frac{\partial \dot{\mathbf{p}}_{F_L} / \partial \mathbf{v}} \right)^\top \\ \left(\frac{\partial \dot{\mathbf{p}}_{F_R} / \partial \mathbf{v}} \right)^\top \\ 0_{2 \times 6} \end{bmatrix}. \quad (7)$$

The vector $\mathbf{u}_t = [\mathbf{u}_{t_L}, \mathbf{u}_{t_R}]^\top$ is formed from the left and thruster forces \mathbf{u}_{t_L} and \mathbf{u}_{t_R} , respectively.

The GRF is modeled using the unilateral compliant ground model with undamped rebound while the friction is modeled using the Stribeck friction model, defined as follows:

$$\begin{aligned} u_{g,z} &= -k_{g,p} p_{F,z} - k_{g,d} \dot{p}_{F,z} \\ u_{g,x} &= - \left(\mu_c + (\mu_s - \mu_c) \exp \left(- \frac{|\dot{p}_{F,x}|^2}{v_s^2} \right) \right) f_z \operatorname{sgn}(\dot{p}_{F,x}) \\ &\quad - \mu_v \dot{p}_{F,x}, \end{aligned} \quad (8)$$

where $p_{F,x}$ and $p_{F,z}$ are the x and z components of the inertial foot position, $k_{g,p}$ and $k_{g,d}$ are the spring and damping model for the ground, μ_c , μ_s , and μ_v are the Coulomb, static, and viscous friction coefficient respectively, and v_s is the Stribeck velocity. $k_{g,d} = 0$ if $\dot{p}_{F,z} > 0$ for the undamped rebound model and the friction in the y direction follows a similar derivation to $u_{g,x}$. Then the ground force model \mathbf{u}_g is defined as follows:

$$\mathbf{u}_g = [\mathbf{u}_{g_L}^\top H(-p_{F_L,z}), \mathbf{u}_{g_R}^\top H(-p_{F_R,z})]^\top, \quad (9)$$

where $H(x)$ is the heaviside function, while \mathbf{u}_{g_L} and \mathbf{u}_{g_R} are the left and right ground forces which are formed using their respective $u_{g,x}$, $u_{g,y}$, and $u_{g,z}$. Finally, the full system equation of motion can be derived using (4) to (9) to form $\dot{\mathbf{x}} = \mathbf{f}(\mathbf{x}, \mathbf{u}_j, \mathbf{u}_t, \mathbf{u}_g)$.

B. Reduced-Order Models

The following reduced-order models are used: a variable length inverted pendulum (VLIP) model and a two-body pendulum model, as illustrated in Fig. 3. The VLIP model is used to describe walking with an ERG, while the two-body pendulum model is used to describe the flight phase with a Model Predictive Control (MPC) to track trajectory and regulate the appropriate leg postures at the time of landing.

1) Variable-Length Inverted Pendulum (VLIP) Model:

As shown in Fig. 3a, the model is described simply using the inverted pendulum model where the length of r can be adjusted through the change in leg conformation. The center of pressure, \mathbf{c} , is defined as the weighted average position of the foot, $\mathbf{c} = \lambda_L \mathbf{p}_{F_L} + \lambda_R \mathbf{p}_{F_R}$, where $\lambda_i = u_{g_i,z} / (u_{g_L,z} + u_{g_R,z})$, $i \in \{L, R\}$. Harpy is modeled using a point foot, so \mathbf{c} is equal to the stance foot position during the SS phase. The VLIP model without thrusters is underactuated, but the

addition of thrusters makes the system fully actuated and enables it to do trajectory tracking.

The dynamic model is derived as follows:

$$m\ddot{\mathbf{p}}_B = m\mathbf{g} + \mathbf{u}_{t,c} + J_s^\top \boldsymbol{\lambda} \quad (10)$$

where m is the mass of the pendulum which in this case is the total mass of the system, and $\mathbf{u}_{t,c}$ is the thruster forces about the body CoM. The constraint force $J_s^\top \boldsymbol{\lambda}$ is setup to keep the leg length r equal to the leg conformation using the following constraint equation:

$$J_s (\ddot{\mathbf{p}}_B - \ddot{\mathbf{c}}) = u_r, \quad J_s = (\mathbf{p}_B - \mathbf{c})^\top, \quad (11)$$

which is designed to keep the leg length second derivative equal to u_r . This constraint force also forms the GRF as long as the friction cone constraint is satisfied. Assuming no slip ($\ddot{\mathbf{c}} = 0$), then the inputs to the system are u_r which controls the body position about the vector $\mathbf{r} = \mathbf{p}_B - \mathbf{c}$ by adjusting the leg length, and the thrusters \mathbf{u}_t which controls the remaining DoFs.

2) *Two-body Pendulum Model*: As shown in Fig. 3b, the model is described as a planar double pendulum in the x - z plane where the mass is concentrated in the body CoM and knee, m_1 and m_2 respectively. Here, the mass of the pelvis motors are combined into the m_1 while the mass of both hips are combined into m_2 to ensure a similar kinematics behavior. The control action is defined as $\mathbf{u}_{dp} = [u_x, u_z, u_h]^\top$ where u_x and u_z are the sum of thruster forces in the x and z directions, respectively, and u_h is the sagittal hip motor torque. The model uses the following states $\mathbf{q}_{dp} = [p_{B,x}, p_{B,z}, q, \theta]^\top$, where q is the hip joint angle and θ is the body absolute pitch angle. Then the system acceleration can be derived as follows:

$$M_{dp}\ddot{\mathbf{q}}_{dp} + \mathbf{h}_{dp} = B_{dp}\mathbf{u}_{dp}, \quad (12)$$

where $B_{dp} = [I_{3 \times 3}, 0_{1 \times 3}]$, allows the direct control signal to the system states except θ .

III. CONTROL OF THRUSTER-ASSISTED LOCOMOTION

This section discusses and outlines the applications of thrusters in our robot, particularly to stabilize the frontal dynamics, apply the ERG framework to regulate GRFs, and to perform ballistic motions to avoid obstacles.

A. Frontal Dynamics Stabilization

In order to show the application of thruster-assisted walking in our robot, we use a walking gait designed for a planar bipedal robot. The absence of the frontal dynamics means that this gait is unstable for 3D walking. Hence the thrusters are used to stabilize the robot's roll and yaw to achieve a stable walking gait in the full 3D system.

The gait is designed by constraining the system dynamics in the x - z plane using 4th order Bezier polynomials to define the feet-end positions relative to the hip in the robot body frame ($\mathbf{p}_F^B - \mathbf{p}_P^B$). Let \mathbf{P}_i , $i \in \{0, \dots, 4\}$ be the Bezier polynomial parameters. This 4th order polynomial can be constrained to have zero initial and final gait velocity by setting $\mathbf{P}_0 = \mathbf{P}_1$ and $\mathbf{P}_3 = \mathbf{P}_4$. Then the free

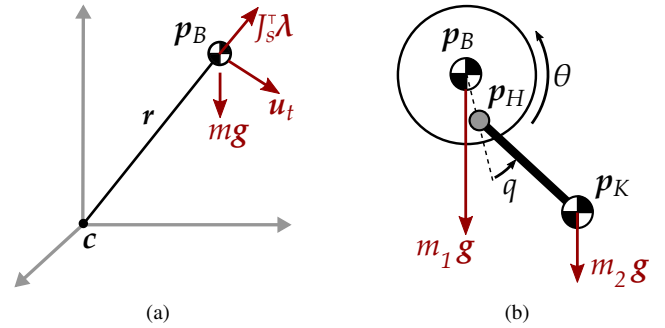


Fig. 3. Illustrates two reduced-order models, a variable-length inverted pendulum (VLIP) and a two-body pendulum model, which are used to describe the dominant dynamic response of the system during the walking and ballistic motions, respectively.

parameters \mathbf{P}_0 , \mathbf{P}_2 , and \mathbf{P}_4 define the initial, middle, and final positions of the gait. Each swing and stance feet-end have a constant Bezier curve parameters to form the 2D open-loop walking gait. The following parameters defined in the x - z plane are used: $\mathbf{P}_{0,sw} = [-0.21, -0.60]^\top \text{m}$, $\mathbf{P}_{2,sw} = [-0.20, -0.50]^\top \text{m}$, and $\mathbf{P}_{4,sw} = [0.10, -0.60]^\top \text{m}$ for the swing foot, and $\mathbf{P}_{0,st} = [0.10, -0.60]^\top \text{m}$, $\mathbf{P}_{2,st} = [0.01, -0.63]^\top \text{m}$, and $\mathbf{P}_{4,st} = [-0.21, -0.60]^\top \text{m}$ for the stance foot. These Bezier parameters define the feet positions and then the joint angles are found simply by resolving the corresponding inverse kinematics problem. Finally, these joint trajectories are tracked using an asymptotically stable controller [35].

The thrusters are used to stabilize the roll and yaw motion of the robot using the following controller

$$\mathbf{u}_{t_{L,F}} = [u_{yaw}, 0, u_{roll}]^\top, \quad \mathbf{u}_{t_{R,F}} = -\mathbf{u}_{t_{L,F}}, \quad (13)$$

where $\mathbf{u}_{t_{L,F}}$ and $\mathbf{u}_{t_{R,F}}$ are the left and right thruster force components for frontal dynamics stabilization, while u_{roll} and u_{yaw} are simple PD controllers to track zero roll and yaw reference angles. This controller is sufficient to stabilize the frontal dynamics and the robot's heading even when using a gait designed for a 2D bipedal robot. During walking, the combined thruster forces are formed by combining $\mathbf{u}_{t,c}$ in (10) and (13), as follows

$$\mathbf{u}_t = [\mathbf{u}_{t,c}^\top, \mathbf{u}_{t,c}^\top]^\top / 2 + [\mathbf{u}_{t_{L,F}}^\top, \mathbf{u}_{t_{R,F}}^\top]^\top. \quad (14)$$

B. Thruster-Assisted Enforcement of GRF Constraints Using RG-based Methods

The ERG framework is utilized to enforce the friction pyramid constraint of the robot by manipulating the applied reference to the controller, which is useful to avoid using optimization or nonlinear MPC framework to enforce constraints on the harder-to-model GRFs. The VLIP model in (10) can be fully actuated due to the addition of thrusters, which enables us to utilize a more advanced controller such as ERG.

The ERG manipulates the applied reference (\mathbf{x}_w) to avoid violating the constraint equation $\mathbf{h}_w(\mathbf{x}, \mathbf{x}_w) \geq 0$ while also be as close as possible to the desired reference (\mathbf{x}_r),

as illustrated in Fig. 4. Consider the Lyapunov equation $V = (\mathbf{x}_r - \mathbf{x}_w)^\top P(\mathbf{x}_r - \mathbf{x}_w)$. \mathbf{x}_w is updated through the update law:

$$\dot{\mathbf{x}}_w = \mathbf{v}_r + \mathbf{v}_t + \mathbf{v}_n, \quad (15)$$

where \mathbf{v}_r drives \mathbf{x}_w directly to \mathbf{x}_r , while \mathbf{v}_t and \mathbf{v}_n drives \mathbf{x}_w along the surface and into the constraint equation boundary $h_w = 0$, respectively. The objective of this ERG algorithm is to drive \mathbf{x}_w to the state $\mathbf{x}_{w,t}$ which is the minimum energy solution V_{min} that satisfies the constraint $h_w \geq 0$.

Let $\mathbf{h}_r(\mathbf{x}, \mathbf{x}_r) = J_r \mathbf{x}_r + \mathbf{d}_r \geq \mathbf{0}$ be the constraint equation using the desired reference \mathbf{x}_r , and C_r be the row space of the violated constraints of \mathbf{h}_r . Define $N_r = \text{null}(C_r) = [\mathbf{n}_1, \dots, \mathbf{n}_n]$ where n is the size of the nullspace. Additionally, let \mathbf{r}_k be the k 'th row of J_r . Then the following update law is used for \mathbf{v}_r , \mathbf{v}_t , and \mathbf{v}_n :

$$\begin{aligned} \mathbf{v}_r &= \hat{\alpha}_r (\mathbf{x}_r - \mathbf{x}_w), & \mathbf{v}_n &= \hat{\alpha}_n \mathbf{r}_k \mathbf{r}_k^\top (\mathbf{x}_r - \mathbf{x}_w) \\ \mathbf{v}_t &= \sum_{k=1}^n \hat{\alpha}_t \mathbf{n}_k \mathbf{n}_k^\top (\mathbf{x}_r - \mathbf{x}_w), \end{aligned} \quad (16)$$

where $\hat{\alpha}$ are scalars defined as follows:

$$\begin{aligned} \hat{\alpha}_r &= \begin{cases} \alpha_r, & \text{if } \min(\mathbf{h}_w) \geq 0 \text{ or } \min(\mathbf{h}_r) \geq 0 \\ 0, & \text{else} \end{cases} \\ \hat{\alpha}_t &= \begin{cases} \alpha_t, & \text{if } \min(\mathbf{h}_w) \geq 0 \text{ or } \min(\mathbf{h}_r) < 0 \\ 0, & \text{else} \end{cases} \\ \hat{\alpha}_n &= \begin{cases} \alpha_n, & \text{if } \min(\mathbf{h}_w) \leq \min(\mathbf{h}_r) < 0 \\ -\alpha_n, & \text{if } \min(\mathbf{h}_r) < \min(\mathbf{h}_w) < 0 \\ 0, & \text{else,} \end{cases} \end{aligned} \quad (17)$$

where α is a positive scalar which determines the rate of convergence.

Assuming $\dot{\mathbf{x}}_r = 0$ and using the update law defined from (16) and (17), we will have $\dot{V} = -2(\mathbf{x}_r - \mathbf{x}_w)^\top Q(\mathbf{x}_r - \mathbf{x}_w)$, with $Q = P(\hat{\alpha}_r I + \sum_{k=1}^n \hat{\alpha}_t \mathbf{n}_k \mathbf{n}_k^\top + \hat{\alpha}_n \mathbf{r}_k \mathbf{r}_k^\top)$. We have the gradient $\dot{V} = 0$ if $\min(\mathbf{h}_w) \leq 0$ and $\mathbf{n}_k \perp (\mathbf{x}_r - \mathbf{x}_w)$, while $\dot{V} < 0$ when $\min(\mathbf{h}_r) \geq 0$ or when $\min(\mathbf{h}_w) \geq 0$. In case both applied reference and target constraints equation are violated, we have $\dot{V} > 0$ which drives the \mathbf{x}_w towards the constraint boundary. This allows the \mathbf{x}_w to converge to $\mathbf{x}_{w,t}$ which is the minimum energy solution that satisfies $h_w \geq 0$ as illustrated in Fig. 4.

The GRF constraints for this robot can be derived from the reduced-order model constraint equation in (11) by applying the ground pyramid constraint. We use the following constraints for the ERG:

$$|u_{g,x}| \leq \mu_s u_{g,z}, \quad |u_{g,y}| \leq \mu_s u_{g,z}, \quad u_{g,z} \geq u_{z,min}, \quad (18)$$

where $[u_{g,x}, u_{g,y}, u_{g,z}]^\top = J_s^\top \boldsymbol{\lambda}$ is the ground reaction force model from (10) and (11). This forms the ground friction pyramid constraint and the minimum ground normal force acting on the leg to ensure that the foot doesn't slip.

C. MPC Design and Control of Robot's Ballistic Motion

The thrusters can also be used to traverse rough terrain by simply flying over obstacles. However, it is not possible to stabilize pitch dynamics due to the thrusters position which

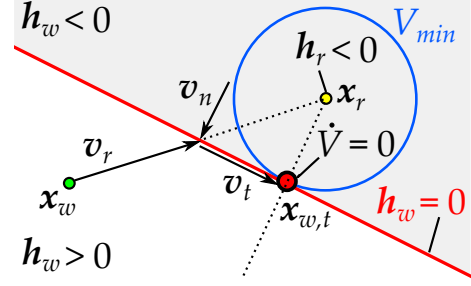


Fig. 4. Shows how an Explicit Reference Governor (ERG) can manipulate the applied reference states \mathbf{x}_w to be as close as possible to the desired reference \mathbf{x}_r while the constraint equations $h_w \geq 0$ remain feasible.

is aligned about the body CoM sagittal axis. Therefore, the reduced-order model in (5) is used to model the robot during the ballistic motion which is represented as a two-body pendulum system. Then an MPC framework is developed based on this model to regulate the feet-end positions and ensuring the proper landing configuration.

The hip frontal and knee angles are setup to be constant during the ballistic maneuver and the feet are positioned in a neutral stance configuration within which legs are parallel to each other. An MPC with a prediction and control horizons $N_h = 10$ is developed using the following optimizer

$$\begin{aligned} \min_{\mathbf{u}_{dp}} & \sum_{k=0}^{N_h} (e^{k\top} W_e e^k + \Delta \mathbf{u}_{dp}^{k\top} W_u \Delta \mathbf{u}_{dp}^k) \Delta t \\ \text{subject to} & \quad \dot{\mathbf{x}}_{dp} = f(\mathbf{x}_{dp}, \mathbf{u}_{dp}) \\ & \quad q_{ref}^{k+1} - \theta^k + q_c = 0 \\ & \quad |\mathbf{u}_{dp}| - \mathbf{u}_{dp,max} \leq 0, \end{aligned} \quad (19)$$

where $e = [\mathbf{p}_B^\top - \mathbf{p}_{B,ref}^\top, q - q_{ref}]^\top$ is the tracking error, W_e and W_u are the cost weighting matrices, and q_c is a constant angle to determine the desired landing posture. q_{ref} denotes the reference hip sagittal angle which is updated each time step relative to the body pitch angle θ and q_c . This reference can ensure the legs do not lag behind the body at the landing moment, and q_c can be properly adjusted to achieve the desired landing posture. The references $\mathbf{p}_{B,ref}$ are designed as a ballistic motion for the body CoM as follows

$$\mathbf{p}_{B,ref}^{k+1} = \mathbf{p}_{B,ref}^k + \Delta t [a, b \sin(2\pi t/1.5)]^\top \quad (20)$$

where \mathbf{p}_B denotes the body position in the x - z plane, while a and b are some constants, and Δt is the controller time step. Finally, the resulting $\mathbf{u}_{dp} = [u_x, u_z, u_h]$ is fed to the full model, where the thruster forces u_x and u_z are combined with the roll and yaw stabilization controller in (13). This forms the combined thruster forces

$$\mathbf{u}_t = [u_x, 0, u_z, u_x, 0, u_z]^\top / 2 + [\mathbf{u}_{t,l}^\top, \mathbf{u}_{t,r}^\top]^\top, \quad (21)$$

which tracks the flight trajectory and stabilizes the robot's roll and heading angles.

IV. SIMULATION RESULTS

The optimization and numerical simulation are done in Matlab where we used interior-point algorithm and RK4 scheme, respectively. The MPC and the ERG filter are

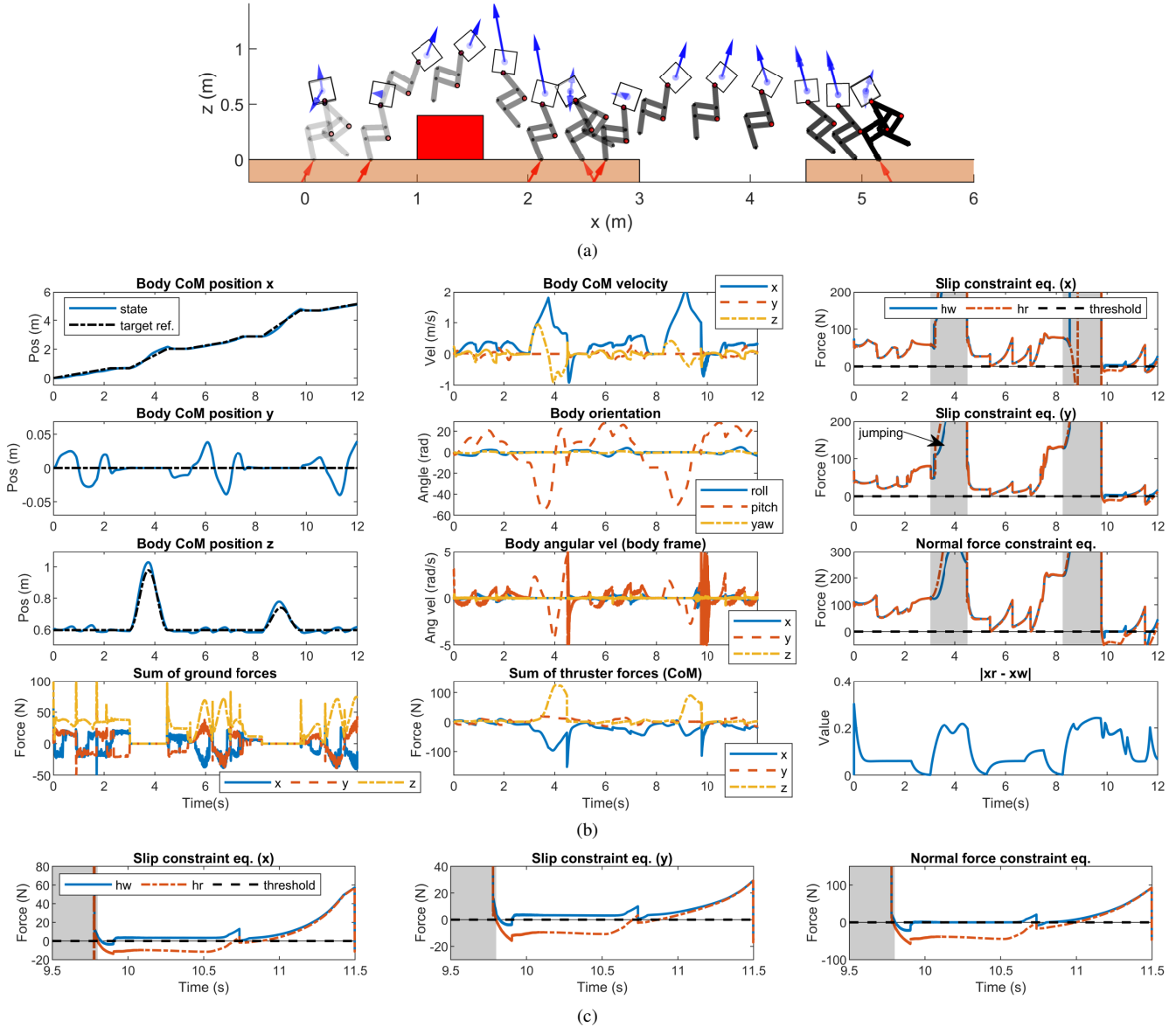


Fig. 5. Shows the simulation result for the walking and jumping maneuvers. (a) Illustrates the stick-diagram plot when the robot walks on flat ground and jumps over obstacles. (b) Depicts the states evolution, the thrusters action and ground contact forces. Note that the thrusters are employed to stabilize the frontal dynamics. The RG algorithm is disabled during the ballistic motion (grey area). (c) Close-up view of the constraints at $t = [9.5, 11.5]$ s where the applied references (\mathbf{x}_w) are manipulated such that the constraints ($\mathbf{h}_w(\mathbf{x}, \mathbf{x}_w) \geq 0$) remain feasible.

simulated using a zero-order hold at a frequency 20 times smaller than the numerical integration to better capture the behavior of the onboard computer in Harpy.

A. Simulation Specifications

In this section, all units are in N, kg, m, s. The robot has the following dimensions: $\mathbf{l}_1 = [0, 0.1, -0.1]^T$, $\mathbf{l}_2 = [0, 0.5, 0]^T$, $\mathbf{l}_3 = [0, 0, -0.3]^T$, and $\mathbf{l}_4 = [0, 0.1, 0]^T$ for the left side. The right side simply has the y axis component inverted. This gives the robot CoM height of around 0.6 m for standing and walking. The following mass and inertias are used: $m_B = 2$, $m_H = m_K = 0.5$, $I_B = 10^{-3}$, $I_H = I_K = 10^{-4}$. Finally, the following ground parameters are used: $\mu_s = 0.6$, $\mu_c = 0.54$, $\mu_v = 0.85$, $k_{g,p} = 8000$,

and $k_{g,d} = 268$. The frequency of MPC controller applied in the two-body pendulum model is 100 Hz with a 10 steps prediction and control horizons. The entire simulation contains 16 gait cycles (12 s) using the following sequence: 3 walking steps, 1 quiet standing cycle, 2 jumping cycles, 4 walking steps, 1 quiet standing cycle, 2 jumping cycles, and 3 walking steps. The weighting matrices for the MPC are $W_e = \text{diag}(5, 20)$, $W_u = \text{diag}(1/10, 1/10, 1/5)$, $q_c = 23^\circ$, and the parameters for the jumping trajectories are $a = 0.9$, $b = 0.8$ for the first jumping cycle, and $a = 1.2$, $b = 0.3$ for the second jump. The ERG is applied using $\alpha = 5$ which provides a sufficient convergence rate.

B. Simulation Results and Discussions

The simulation results can be seen in Fig. 5, where Fig. 5a shows the key frames of the simulated robot trajectory where it walks and jumps over obstacles. Figure 5b shows the data of the thruster forces, ground normal forces, and body states during the simulation. The walking gait designed for a 2D bipedal robot is stable when used in the full 3D system as the pitch and yaw angles are stabilized by the thruster actions. Additionally, the trajectory of the body positions match closely towards the desired trajectories throughout the walking and flight phases. The robot's pitch angle is uncontrollable as shown in Fig. 5b throughout the entire simulation. However, the MPC has successfully regulated the foot landing positions such that the foot is positioned below or in front of the body at the time of landing through the appropriate hip sagittal angles, as shown in Fig. 5a. This allows a smooth transition between landing and walking which is the primary objective of using the MPC.

The ERG is used to regulate the ground friction forces by manipulating the applied state references during walking to prevent slips. Figure 5b shows the constraint equation values using the applied and target reference (\mathbf{h}_w and \mathbf{h}_r respectively), where the target reference trajectories satisfy the constraints except at around the time range of $t = [10, 12]$ s as shown in Fig. 5c. Within this time range, the desired reference trajectory results in $\min(\mathbf{h}_r) < 0$ and the ERG has successfully manipulate the applied reference \mathbf{x}_w such that the constraint equation $\mathbf{h}_w \geq 0$ is satisfied. The control output of the ERG is disabled during the jumping period (shaded gray in Fig. 5b) as the thruster components for position stabilization is handled by the MPC.

V. CONCLUSIONS AND FUTURE WORK

The concept design and dynamics simulation of a thruster-assisted bipedal robot called Harpy is presented in this paper. The addition of the thrusters allows the robot to stabilize its frontal dynamics easily and be able to regulate the ground contact forces directly. To do this, a control algorithm based on Reference Governors (RGs) was proposed. In addition, the thrusters allowed multimodal locomotion where the robot can transition between walking and jumping over obstacles. Through simulations we showed that the integration of the thrusters can yield a dynamically robust biped. Future work includes the completion of Harpy. In addition, we will explore the cost of transport in multi-modal systems. Further investigations will be made in developing high fidelity models that incorporate realistic thruster dynamics which are more appropriate for the real-world implementation of closed-loop feedback on Harpy.

REFERENCES

- [1] M. H. Raibert, H. B. Brown Jr, and M. Chepponis, "Experiments in balance with a 3d one-legged hopping machine," *The International Journal of Robotics Research*, vol. 3, no. 2, pp. 75–92, 1984.
- [2] M. Raibert, K. Blankespoor, G. Nelson, and R. Playter, "Bigdog, the rough-terrain quadruped robot," *IFAC Proceedings Volumes*, vol. 41, no. 2, pp. 10822–10825, 2008.
- [3] Y. Gong, R. Hartley, X. Da, A. Hereid, O. Harib, J.-K. Huang, and J. Grizzle, "Feedback control of a cassie bipedal robot: Walking, standing, and riding a segway," in *2019 American Control Conference (ACC)*, 2019, pp. 4559–4566.
- [4] M. Hirose and K. Ogawa, "Honda humanoid robots development," *Philosophical Transactions of the Royal Society A: Mathematical, Physical and Engineering Sciences*, vol. 365, no. 1850, pp. 11–19, 2006.
- [5] W. Kwon *et al.*, "Biped humanoid robot mahru iii," in *IEEE-RAS International Conf. on Humanoid Robots*. IEEE, 2007, pp. 583–588.
- [6] J. E. Pratt *et al.*, "The yobotics-ihmc lower body humanoid robot," in *IEEE/RSJ International Conference on Intelligent Robots and Systems*, 10 2009, pp. 410–411.
- [7] H.-W. Park, A. Ramezani, and J. W. Grizzle, "A finite-state machine for accommodating unexpected large ground-height variations in bipedal robot walking," *IEEE Transactions on Robotics*, vol. 29, no. 2, pp. 331–345, 2012.
- [8] B. G. Buss, A. Ramezani, K. A. Hamed, B. A. Griffin, K. S. Galloway, and J. W. Grizzle, "Preliminary walking experiments with underactuated 3d bipedal robot marlo," in *2014 IEEE/RSJ International Conference on Intelligent Robots and Systems*, 2014, pp. 2529–2536.
- [9] H.-W. Park, K. Sreenath, A. Ramezani, and J. W. Grizzle, "Switching control design for accommodating large step-down disturbances in bipedal robot walking," in *2012 IEEE International Conference on Robotics and Automation*, 2012, pp. 45–50.
- [10] G. Picardi, H. Hauser, C. Laschi, and M. Calisti, "Morphologically induced stability on an underwater legged robot with a deformable body," *The International Journal of Robotics Research*, 2019.
- [11] Y. Kojio *et al.*, "Walking control in water considering reaction forces from water for humanoid robots with a waterproof suit," in *2016 IEEE/RSJ International Conference on Intelligent Robots and Systems (IROS)*, 2016, pp. 658–665.
- [12] B. Araki, J. Strang, S. Pohorecky, C. Qiu, T. Naegeli, and D. Rus, "Multi-robot path planning for a swarm of robots that can both fly and drive," in *2017 IEEE International Conference on Robotics and Automation (ICRA)*, 2017, pp. 5575–5582.
- [13] E. Westervelt and J. Grizzle, *Feedback Control of Dynamic Bipedal Robot Locomotion*, ser. Control and Automation Series. CRC Press/INC, 2007.
- [14] K. Galloway, K. Sreenath, A. D. Ames, and J. W. Grizzle, "Torque saturation in bipedal robotic walking through control lyapunov function-based quadratic programs," *IEEE Access*, vol. 3, pp. 323–332, 2015.
- [15] H. Dai and R. Tedrake, "Planning robust walking motion on uneven terrain via convex optimization," in *IEEE-RAS International Conference on Humanoid Robots (Humanoids)*, 11 2016, pp. 579–586.
- [16] S. Feng, E. Whitman, X. Xinjilefu, and C. G. Atkeson, "Optimization based full body control for the atlas robot," in *IEEE-RAS International Conference on Humanoid Robots*, 11 2014, pp. 120–127.
- [17] A. Ramezani, J. W. Hurst, K. Akbari Hamed, and J. W. Grizzle, "Performance analysis and feedback control of atrias, a three-dimensional bipedal robot," *Journal of Dynamic Systems, Measurement, and Control*, vol. 136, no. 2, 2014.
- [18] A. Ramezani, "Feedback control design for marlo, a 3d-bipedal robot." Ph.D. dissertation, 2013.
- [19] J. Grizzle, A. Ramezani, B. Buss, B. Griffin, K. A. Hamed, and K. Galloway, "Progress on controlling marlo, an atrias-series 3d underactuated bipedal robot," *Dynamic Walking*, 2013.
- [20] P. Dangol, A. Ramezani, and N. Jalili, "Performance satisfaction in midget, a thruster-assisted bipedal robot," in *2020 American Control Conference (ACC)*, 2020, pp. 3217–3223.
- [21] A. C. de Oliveira and A. Ramezani, "Thruster-assisted center manifold shaping in bipedal legged locomotion," in *2020 IEEE/ASME International Conference on Advanced Intelligent Mechatronics (AIM)*. IEEE, 2020, pp. 508–513.
- [22] P. Dangol and A. Ramezani, "Towards thruster-assisted bipedal locomotion for enhanced efficiency and robustness," *International Federation of Automatic Control (IFAC)*, 2020.
- [23] A. Hereid, E. A. Cousineau, C. M. Hubicki, and A. D. Ames, "3d dynamic walking with underactuated humanoid robots: A direct collocation framework for optimizing hybrid zero dynamics," in *2016 IEEE International Conference on Robotics and Automation (ICRA)*, 2016, pp. 1447–1454.
- [24] L. Sentis and O. Khatib, "A whole-body control framework for humanoids operating in human environments," in *Proceedings 2006*

- IEEE International Conference on Robotics and Automation, 2006. ICRA 2006.*, 2006, pp. 2641–2648.
- [25] W. B. Powell, *Approximate Dynamic Programming: Solving the curses of dimensionality*. John Wiley & Sons, 2007, vol. 703.
 - [26] R. S. Sutton and A. G. Barto, *Reinforcement learning: An introduction*. MIT press, 2018.
 - [27] M. Rafieisakhaei, S. Chakravorty, and P. Kumar, “A near-optimal decoupling principle for nonlinear stochastic systems arising in robotic path planning and control,” in *2017 IEEE 56th Annual Conference on Decision and Control (CDC)*, 2017, pp. 1–6.
 - [28] E. D. Sontag, “A Lyapunov-like characterization of asymptotic controllability,” *SIAM journal on control and optimization*, vol. 21, no. 3, pp. 462–471, 1983.
 - [29] P. V. Kokotovic, M. Krstic, and I. Kanellakopoulos, “Backstepping to passivity: recursive design of adaptive systems,” in *IEEE Conference on Decision and Control*, vol. 4, 12 1992, pp. 3276–3280.
 - [30] S. P. Bhat and D. S. Bernstein, “Continuous finite-time stabilization of the translational and rotational double integrators,” *IEEE Transactions on Automatic Control*, vol. 43, no. 5, pp. 678–682, 1998.
 - [31] E. Garone and M. M. Nicotra, “Explicit reference governor for constrained nonlinear systems,” *IEEE Transactions on Automatic Control*, vol. 61, no. 5, pp. 1379–1384, 2015.
 - [32] E. G. Gilbert, I. Kolmanovsky, and Kok Tin Tan, “Nonlinear control of discrete-time linear systems with state and control constraints: a reference governor with global convergence properties,” in *IEEE Conference on Decision and Control*, vol. 1, 12 1994, pp. 144–149.
 - [33] A. Bemporad, “Reference governor for constrained nonlinear systems,” *IEEE Trans. on Automatic Control*, vol. 43, no. 3, pp. 415–419, 1998.
 - [34] E. Gilbert and I. Kolmanovsky, “Nonlinear tracking control in the presence of state and control constraints: a generalized reference governor,” *Automatica*, vol. 38, no. 12, pp. 2063–2073, 2002.
 - [35] H. Khalil, *Nonlinear Systems*. Pearson Education, Prentice Hall, 2002.